Climate Dynamics (2000) 16:789–797

G. L. Russell · V. Gornitz · J. R. Miller

Regional sea level changes projected by the NASA/GISS Atmosphere-Ocean Model

Received: 22 November 1999 / Accepted: 20 April 2000

Abstract Sea level has been rising for the past century, and coastal residents of the Earth will want to understand and predict future sea level changes. In this study we present sea level changes from new simulations of the Goddard Institute for Space Studies (GISS) global atmosphere-ocean model from 1950 to 2099. The free surface, mass conserving ocean model leads to a straightforward calculation of these changes. Using observed levels of greenhouse gases between 1950 and 1990 and a compounded 0.5% annual increase in CO_2 after 1990, model projections show that global sea level measured from 1950 will rise by 61 mm in the year 2000, by 212 mm in 2050, and by 408 mm in 2089. By 2089, 64% of the global sea level rise will be due to thermal expansion and 36% will be due to ocean mass changes. The Arctic Ocean will show a greater than average sea level rise, while the Antarctic circumpolar region will show a smaller rise in agreement with other models. Model results are also compared with observed sea level changes during the past 40 years at 12 coastal stations around the world.

1 Introduction

During the last century, sea level has been rising throughout much of the world at rates between 1 and 2.5 mm/year with a best estimate of 1.8 mm/year (Warrick et al. 1996; Gornitz 1995a). Increasing levels of atmospheric greenhouse gases are mainly responsible for the present global sea level rise and its future continuation. There are two major components to long term sea level changes: first, water expands as ocean temperatures change and salt is redistributed; and second, land ice stored on the continents and in polar ice sheets melts and flows into the oceans. At any coastal location, vertical land motions may also affect local mean sea level. Locally, we will use the term "steric expansion" for a combination of thermal and haline expansion; whereas globally, we will simply use "thermal expansion" because the global effect of haline expansion is negligible.

Several prior studies have modeled potential changes in sea level in coupled atmosphere-ocean models. Cubasch et al. (1995) coupled the atmospheric component (ECHAM-1) and the large-scale geostrophic ocean model (LSG) in a warm start simulation with the radiative forcing similar to the IS92a scenario (slightly weaker than 1% CO_2 annual increases) from the Intergovernmental Panel on Climate Change (IPCC) (Houghton et al. 1992). The global sea level rise due to thermal expansion was 180 mm after 100 years. In a companion cold start simulation, the sea level rise was only 150 mm. Bryan (1996) used the Geophysical Fluid Dynamics Laboratory coupled model in a 1% CO_2 annual increase simulation. After 70 years, global sea level rose 150 mm due to thermal expansion alone. Gregory and Lowe (2000) evaluated sea level changes using two Hadley Centre coupled models, HadCM2 and HadCM3. HadCM3, which uses the IPCC IS92a scenario for greenhouse gas emissions, predicted a global sea level rise of 440 mm from 1990 to 2100, of which 60% resulted from thermal expansion.

Other studies have used one or two dimensional models to examine both thermal expansion and water mass changes that cause sea level to rise. Raper et al. (1996) combined a simple one dimensional upwelling-diffusion energy balance model with a set of simple ice-melt models in order to compute total sea level change. Using the IPCC 1995 suite of greenhouse gas emissions scenarios (Houghton et al. 1996), they found a sea level rise of 200–860 mm from year 1990 to 2100, with a mid value of 490 mm for a climate sensitivity of 2.5 °C for doubled CO_2. De Wolde et al. (1997) applied a two dimensional energy balance climate model and dynamic

G. L. Russell (✉) · V. Gornitz · J. R. Miller
NASA/Goddard Institute for Space Studies,
2880 Broadway, New York, NY 10025, USA
E-mail: grussell@giss.nasa.gov

ice sheet models to the IPCC forcing scenarios to estimate sea level rise contributions from thermal expansion and glacial melting. Their results were considerably lower than those of the IPCC (Warrick et al. 1996). Sea level rise projections showed a strong sensitivity to differences in model features.

In this study, we use the global coupled atmosphere-ocean model of Russell et al. (1995) to examine sea level rise between 1950 and 2099. Since the model has a free surface and conserves global water mass in all phases, the ocean surface height can be calculated directly by integrating specific volume with respect to mass from the ocean floor. The model is described in Sect. 2. Four 150-year model simulations used in the analysis are discussed in Sect. 3. In Sect. 4, the results are compared with observed changes at 12 coastal stations from 1960 to 1998. In Sect. 5, the model is used to project sea level changes to the end of the twenty first century. A breakdown of the water mass changes is performed in Sect. 6.

2 The NASA/GISS atmosphere-ocean model

The global synchronously coupled atmosphere-ocean model developed by Russell et al. (1995) is designed for climate studies on decade to century time scales. There are nine vertical layers in the atmosphere and 13 in the ocean. The horizontal resolution for both the atmosphere and ocean is 4° in latitude by 5° in longitude. The resolution for heat, water vapor, and salt is finer than the grid resolution because those quantities have both means and directional prognostic gradients inside each grid cell. This information is used in the advection by the linear upstream scheme, and atmospheric condensation and ocean vertical mixing are performed on $2° \times 2.5°$ horizontal resolution. The model does not use flux adjustments.

Several changes and improvements have been made to the model since it was published. The ground hydrology scheme of Abramopoulos et al. (1988) is now implemented; land ice and sea ice coding uses four thermodynamic layers; sea ice is advected; glacial ice calving is implemented off Antarctica; and the k-profile parametrization (KPP) scheme (Large et al. 1994) is used for ocean vertical mixing. Before the KPP scheme was implemented, the equilibrium surface air temperature change due to doubled CO_2 was estimated to be 2.65 °C (Andrei Sokolov and Peter Stone personal communication).

The ocean model does not use the Boussinesq approximation, and ocean mass, not volume, is conserved. As part of the ocean pressure gradient force, height is calculated by integrating the local specific volume with respect to mass per unit area from the ocean floor. The specific volume is calculated with quadratic precision in each layer using the mean and vertical gradients of heat and salt. The ocean surface height, which is sampled each hour, is the summation of the liquid ocean surface height plus the snow and sea ice mass per unit area divided by a constant density of 1000 kg/m^3 which measures the freshwater equivalent of snow and ice.

Solid, liquid and gas phases of water are prognostic variables of the model, so the ocean column mass at any location is simply the summation of the correct prognostic variables. In any column, ocean mass varies due to transport, decreases due to evaporation, and increases due to precipitation, river flow including melted ice, and glacial ice calving from Antarctica. Salt varies due to transport, but is conserved globally. Global ocean mass changes are compensated by global changes in atmospheric or continental water reservoirs. Local changes in wind stress and ocean circulation are reflected in local ocean mass changes.

Change in ocean surface height due to steric expansion between any ocean states or monthly averages is calculated as the change in ocean surface height minus the ocean mass change divided by a constant density of 1000 kg/m^3. This calculation of steric expansion is consistent with Bryan's (1996, Eq. 3) "dynamic topography anomaly" when integrated over the same vertical extent.

The model calculates snow accumulation and melting on land ice. Rain or meltwater has the chance to refreeze in any lower ice layer (if its temperature is below 0 °C) before it eventually finds its way back to the ocean via the river network. Land ice reservoirs on whole or fractional continental grid cells can melt or accumulate ice indefinitely, but the changes are captured by the model's diagnostics. Land ice areas are constant in time; regional areas are shown in Table 4. Mountain glaciers and small ice caps are underrepresented by the model by 40% whereas the model's area of Greenland land ice is too large (Warrick et al. 1996, Table 7.1). The model has no land ice in the Himalayas or South America.

Land ice calving from Antarctica was determined from an atmospheric model simulation that used current climatological ocean temperatures and sea ice cover. Local mass balance was calculated from precipitation minus evaporation minus meltwater (Antarctica had very little). Assuming that Antarctica is currently in equilibrium, the local mass balance must be compensated by horizontal land ice transport using the river network directions. Land ice transport that reaches the coast is pushed into and melts in the ocean in the coupled model. The constant annual discharge by the model is $2986 \cdot 10^{12}$ kg/year which is greater than $2016 \cdot 10^{12}$ that was estimated by Warrick et al. (1996, Table 7.1). Land ice calving was not implemented in Greenland because some Northern Hemisphere ice basins are losing mass (although more are gaining) and because the Greenland imbalance was much less than the Antarctic imbalance.

Snow over ground increases indefinitely at certain cold grid cells. Continual long term changes of water mass between a control simulation and a model experiment over ground are mainly due to snow changes because canopy and underground water storage are limited. Negative lake mass changes may occur by excessive evaporation from the surface area of a lake that does not receive sufficient precipitation, source runoff from within its grid cell, or river flow from upstream lakes. Positive lake mass changes may occur when water sources exceed evaporation (the surface area may be negligible) and there is no or slow outgoing river flow. In the model, lakes occupy 0.8% of the global surface area and are fixed.

3 Model simulations

Four simulations of the atmosphere-ocean model from 1950 to 2099 are used in this study: two control simulations with constant 1950 atmospheric composition that differ only in their initial conditions, and two GHG experiments with observed greenhouse gases until 1990 and 0.5% compounded annual increases of CO_2 after 1990. In addition, two GHG + SO_4 experiments with varying tropospheric sulfate aerosols were run; but because their temperature comparisons did not agree as well with observations as did the GHG experiments (Russell et al. 2000), they have not been included here. The radiative forcing of 0.5% CO_2 annual increases is in line with the radiative forcing of all greenhouse gas increases for the past few years (Hansen et al. 1998). This forcing rate is less than the IPCC's scenario IS92a and is less than the forcing rate used by other groups that have studied sea level rise. The initial conditions are 40-year and 100-year spinups with constant 1950 atmospheric composition starting from Levitus et al.'s (1994) ocean state. In order to minimize climate drift (continual accumulation of heat or salt at certain locations) and deviations from observations, model climate changes are calculated as an experiment minus a control simulation.

Russell et al. (2000) compared these current simulations with the observed regional temperature record of the past 40 years and concluded that the model faithfully represents the real world's regional climate changes due to greenhouse gas forcing in the Northern Hemisphere. They estimated that the unrealized warming in surface air temperature due to the cold start initialization is 0.23 °C, but because the 1930s and 1940s were anomalously warm

decades, the surface air temperature disparity with observations is negligible. Although the cold start initialization may not be detectable in the surface air temperature, it should be present in the deep ocean temperatures and ocean surface height. Consequently, the model's sea level changes probably underestimate those that occur in the real world.

Cubasch et al. (1995), using observed greenhouse gas concentrations from 1935 to 1985 followed approximately by IS92a in their coupled model simulations, estimated that using a warm start for 50 years prior to 1985 versus a cold start in 1985 added 30 mm to the sea level rise by 2085. The change in radiative forcing due to greenhouse gases from 1935 to 1985 is 1.6 times that from 1850 to 1950. Thus, our model's underestimation of global sea level rise by thermal expansion caused by unrealized warming from 1850 to 1950 may be about 30/1.6 = 19 mm in the twenty first century.

4 Model and observed sea level trends at coastal stations

Observations of sea level rise are obtained from tide gauges at coastal stations. Model data are used from whole ocean grid cells that are nearest to the station. Although the model's resolution is coarse and the relationship between an area averaged sea level height and a tide gauge point measurement is unclear, we put on the same graph tide gauge records for the past century and sea level predictions for the next century.

Monthly raw tide gauge data are obtained from the Permanent Service for Mean Sea Level (PSMSL) data base (Spencer and Woodworth 1993). Some records go back more than 100 years, but most records are too short or too broken to be useful for sea level studies (Gornitz 1995a). A small subset of 12 tide gauge stations were selected for comparison with model generated sea level curves. These stations were chosen on the basis of record length, geographical coverage, and availability of adequate geologic data (Gornitz 1995b; Gornitz and Solow 1991; Gornitz and Lebedeff 1987; Pirazzoli 1991). Missing monthly tide gauge data are filled in by interpolation between the same months in prior and subsequent years with a maximum gap of two missing years. Annual data are calculated whenever original or filled in data are available for all 12 months; otherwise an annual data gap occurs.

For each station, tide gauge annual values are normalized by calculating a 21 year mean, centered on 1950, and then subtracting this mean from each annual value. Finally, the geologic trend or vertical land motion is subtracted from the normalized annual values to obtain the corrected sea level change relative to 1950 that can be compared with model results.

Sea level data recorded by tide gauges include long term trends caused by vertical crustal motions largely of glacial isostatic or tectonic origin (Peltier and Tushingham 1991; Gornitz 1995a, b). The late Holocene (past 6000 years) sea level curve constructed from fossil tide level indicators, such as peat, coral, in-situ shells, barnacles, etc., represents a composite of these long term geologic components. The long term geologic motion can be approximated by a linear trend over the relatively short time periods considered here. By differencing the modern and late Holocene sea level curves, the residual provides a measure of the recent sea level rise due to global warming (Gornitz 1995b).

Table 1 lists the station names, latitude, longitude, years of record, the filled uncorrected tide gauge trend (mm/year) for all years of the record, the geologic trend due to land motions, the corrected tide gauge trend for all years of the record, the corrected tide gauge trend for years 1960 to present, and the model sea level trends for each GHG experiment minus its control from 1960 until the end of the observational record. The trends are calculated as the slope of the least squares fit line through the annual sea level data. Note the negative geologic trend in Table 1 at Stockholm which is undergoing glacial isostatic uplift, and the positive value at New York due to subsidence of the collapsed forebulge (Peltier and Tushingham 1991; Peltier 1999).

For each of the 12 stations, Fig. 1 shows the sea level changes for all years of the corrected tide gauge data and for 1960 to 2089 of each GHG experiment. A GHG data point consists of a GHG annual value minus a centered 21 year moving average of the control simulation values. Subtracting control simulation values reduces the effects of climate drift, and the 21 year averaging period lets the GHG data show its proper interannual variability.

Table 1 shows that between 1960 and 1998 the modeled sea level trends are positive at all 12 stations and are generally greater than the corrected tide gauge trends. The global mean sea level trends of 1.41 and 1.39 mm/year for the two GHG experiments between 1960 and 1998 fall within the observed range (Warrick et al. 1996; Gornitz 1995a), but the average of the 12 corrected tide gauge trends lie at the lower end of this range due to the limited sampling of the stations reported here.

It seems unlikely that the corrected tide gauge multi-year trends are representing only anthropogenic global warming trends. A large source of interannual variability in sea level data comes from the El Nino-Southern Oscillation (ENSO) (Nerem 1999) or the North Atlantic Oscillation (NAO) (Hurrell 1995). ENSO and NAO anomalies appear in tide gauge records (Komar and Enfield 1987; Maul and Hanson 1991; Gornitz unpublished data). The sharp positive spike in 1982 in the San Francisco sea level curve (Fig. 1) is related to ENSO, as are lesser anomalies in 1941, 1958, 1969 and 1972. The sharp positive sea level anomaly in 1983 in the Buenos Aires sea level curve may also be linked to ENSO.

Table 1 Tide gauge station name, longitude, latitude, years of record, filled uncorrected tide gauge trend (mm/year) for all years of the record (Spencer and Woodworth 1993), geologic trend due to land motions, corrected tide gauge trend for all years of the record, corrected tide gauge trend for years 1960 to present, and model sea level trends for each GHG experiment minus its control from 1960 until the end of the observational record. Trends, other than the geologic trend, are calculated from a least squares fit line of the data in Fig. 1

City	Longitude, Latitude	Ymin	Ymax	Raw tide	Geologic trend	Corrected all	Corrected 1960	GHG1	GHG2
Auckland	175°E, 35°S	1904	1988	1.35	−0.1	1.45	0.01	1.68	1.78
Bombay	73°E, 19°N	1878	1993	0.75	0.0	0.75	0.22	2.09	1.90
Brest	5°W, 48°N	1807	1996	0.96	0.15	0.81	0.94	1.53	2.46
Buenos Aires	58°W, 35°S	1905	1987	1.57	0.0	1.57	4.79	1.55	2.07
Honolulu	158°W, 21°N	1905	1997	1.55	0.3	1.25	1.33	0.52	0.99
Key West	82°W, 25°N	1913	1997	2.23	0.69	1.54	1.99	1.44	1.33
Marseilles	5°E, 43°N	1885	1996	1.22	0.75	0.47	−1.01	1.18	1.80
New York	74°W, 41°N	1856	1996	2.72	2.17	0.55	0.09	2.53	1.91
San Francisco	122°W, 38°N	1855	1997	1.41	1.5	−0.09	1.14	1.40	1.75
Stockholm	18°E, 59°N	1889	1998	−3.89	−4.5	0.61	1.69	2.95	2.83
Sydney	151°E, 34°S	1897	1993	0.68	−0.3	0.98	1.04	0.76	2.74
Victoria	124°W, 48°N	1910	1996	0.74	0.0	0.74	1.02	1.16	1.50

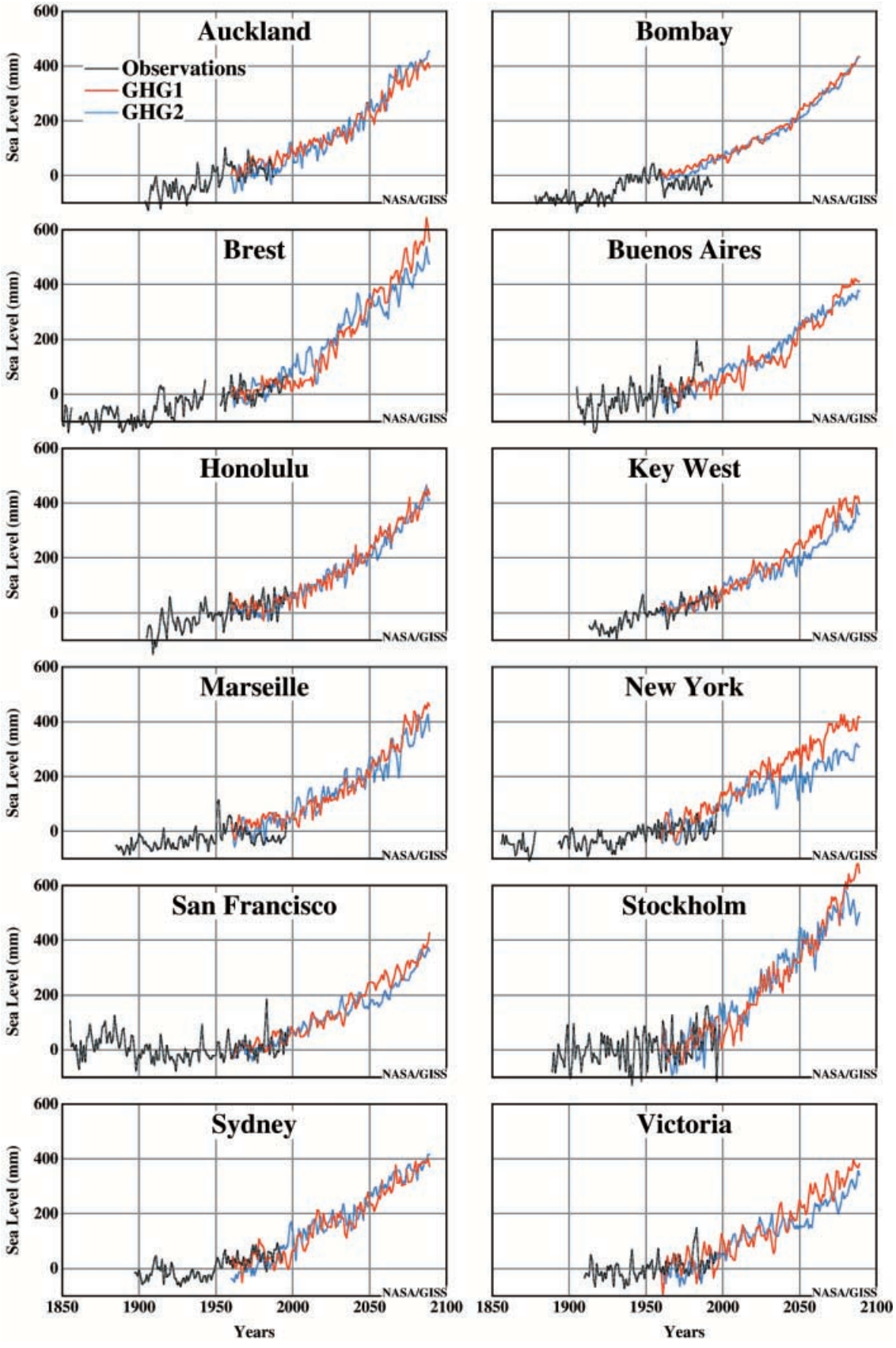
Auckland
Observations
GHG1
GHG2
Bombay
Brest
Buenos Aires
Honolulu
Key West
Marseille
New York
San Francisco
Stockholm
Sydney
Victoria
Sea Level (mm)
600
400
200
0
NASA/GISS
1850
1900
1950
2000
2050
2100
Years

◀

Fig. 1 Graphs for each of 12 stations show sea level changes integrated from 1950 for corrected tide gauge record and for each GHG experiment minus a 21 year moving average of its control. The geologic trend must be added to these graphs to estimate sea level changes at the stations

In general, the model's interannual variability in Fig. 1 appears to be less than that of the observations, although stations with large (small) model variability, such as Stockholm (Bombay), also display large (small) observational variability. The model's ENSO strength is known to be considerably weaker than the real world's. However, ENSO and NAO cannot fully explain the large range of corrected tide gauge trends and the smaller range in the model's sea level trends.

5 Modeled sea level changes to the year 2099

Figure 2 shows the temporal change in global sea level from 1960 to 2089 for the two GHG experiments minus the controls. It also shows the fractions due to thermal expansion and to water mass changes. These data are also recorded in Table 2 in a format consistent with Tables 3 and 4. The fourth line of Table 2, shows the difference in heat that enters the ocean between the GHG experiments and the control simulations. The ratio of global sea level rise due to thermal expansion (mm/year) divided by the heat entering the ocean (W/m^2) gives the "expansion efficiency of heat" ($m^3/kW{\cdot}year$), the final line of Table 2. Note that the model's expansion efficiency for the first 50 years was greater than for the next century. As the warming penetrates more deeply into colder waters, the expansion is less efficient.

The expansion efficiency of heat can be calculated from known ocean variables (Fofonoff and Millard 1983) as the derivative of specific volume with respect to temperature (m^3/kg °C) divided by specific heat capacity

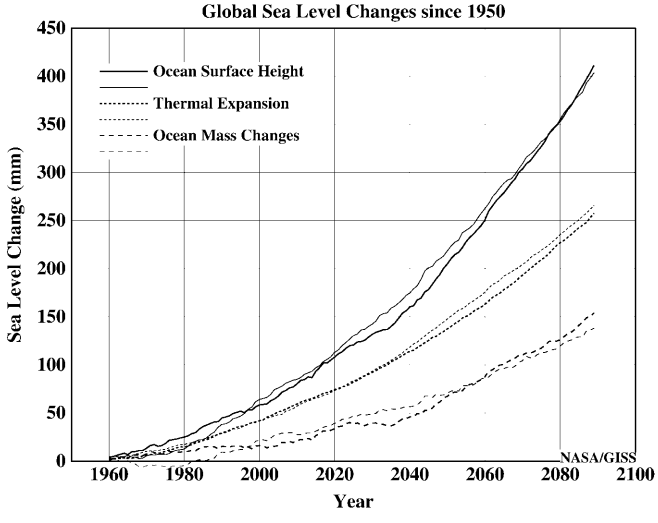

Fig. 2 Integrated annual change in global sea level for each GHG experiment minus a 21 year moving average of its control. Also shown are components due to thermal expansion and to water mass changes

Table 2 Changes in ocean surface height (mm/year) and its components for each GHG experiment minus the appropriate control simulation. The fourth line is the change in net heat into the ocean (W/m^2). The fifth line is the expansion efficiency of heat ($m^3/kW{\cdot}year$), calculated as the ratio of the second and fourth lines

	1950–1999		2000–2049		2050–2099	
	GHG1	GHG2	GHG1	GHG2	GHG1	GHG2
Ocean surface height	1.15	1.29	2.83	3.04	5.55	4.95
Thermal expansion	0.83	0.81	1.91	2.13	3.17	3.00
Water mass change	0.32	0.47	0.92	0.90	2.39	1.95
Net heat into ocean	0.55	0.51	1.36	1.45	2.19	2.05
Expansion efficiency	1.50	1.59	1.41	1.47	1.45	1.47

Table 3 Changes in global water reservoirs in units of sea level rise (mm/year) for each GHG experiment minus the appropriate control simulation

	1950–1999		2000–2049		2050–2100	
	GHG1	GHG2	GHG1	GHG2	GHG1	GHG2
Water vapor	0.03	0.03	0.03	0.05	0.04	0.06
Snow on ground	−0.08	−0.13	−0.41	−0.12	−0.42	−0.23
Land ice	−0.24	−0.40	−0.76	−1.02	−2.33	−2.17
Lake mass	−0.02	0.02	0.23	0.20	0.30	0.37
Ocean + sea ice	0.32	0.47	0.92	0.90	2.39	1.95

(J/kg °C). Figure 3 shows the expansion efficiency as a function of temperature and pressure at a salinity of 35 psu. The expansion efficiency of heat increases with temperature, pressure or salinity.

Bryan (1996) provided a rough estimate of an additional 3 W/m^2 entering his model's ocean for years 50 to 70 in his 1% CO_2 experiment. From his Fig. 2a, we estimate a sea level rise due to thermal expansion of 3.47 mm/year for those two decades which translates into an expansion efficiency of 1.16 $m^3/kW{\cdot}year$. Either his heating rate is only approximate, or his heat is penetrating into colder waters than in our experiments.

The additional heat of Table 2 in the GHG experiments for years 2050 to 2099 enters the ocean at middle and high latitudes as shown in Fig. 4a. Figure 4b shows that the poleward transport of heat by the oceans has been reduced for years 2050 to 2099 as compared with 1950. These figures can be compared with Fig. 6a, b of Bryan (1996).

Figure 5 shows the spatial distribution of projected sea level rise for 2050 to 2099 minus 1950. It was calculated as the 50 year average of the two GHG experiments minus the 50 year average of the two control simulations. The largest rise in sea level occurs in the Arctic Ocean where increased river flow (due to increased precipitation) and decreased sea ice export cause the salinity to

Table 4 Changes in land ice reservoirs in units of sea level rise (mm/year) for each GHG experiment minus the appropriate control simulation. Area is in units of 10^{12} m^2

	Area	1950–1999		2000–2049		2050–2099	
		GHG1	GHG2	GHG1	GHG2	GHG1	GHG2
Antarctica	13.677	−0.083	0.075	−0.237	0.145	−0.188	−0.477
Greenland	1.930	0.003	−0.355	−0.327	−0.666	−1.321	−1.011
Alaska	0.080	−0.076	−0.051	−0.129	−0.218	−0.312	−0.221
Canadian Arctic	0.240	−0.057	−0.088	−0.104	−0.220	−0.358	−0.373
Iceland	0.020	−0.016	0.009	0.056	0.013	−0.024	0.055
Spitzbergen	0.035	−0.016	0.008	−0.024	−0.071	−0.133	−0.148
Novaya Zemlya	0.025	0.001	−0.001	0.001	0.002	0.002	0.003
World	16.008	−0.244	−0.403	−0.763	−1.015	−2.334	−2.173

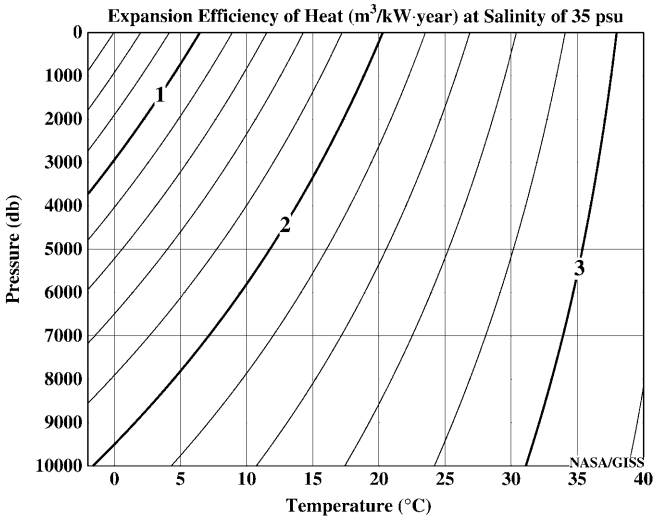

Fig. 3 Expansion efficiency of heat as a function of temperature and pressure at a salinity of 35 psu

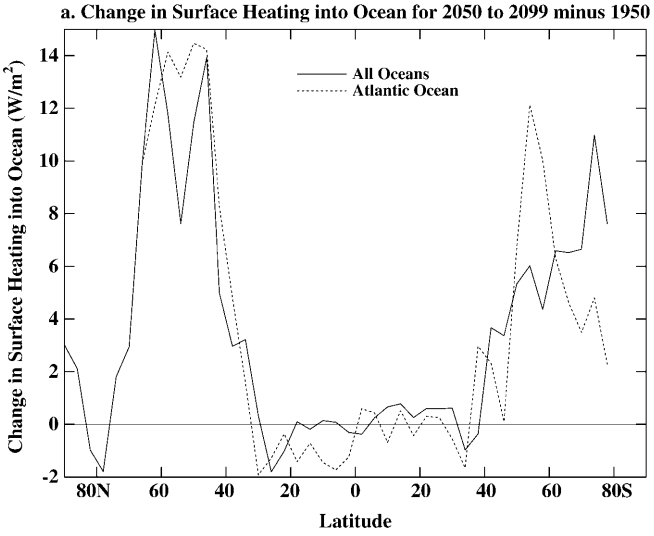

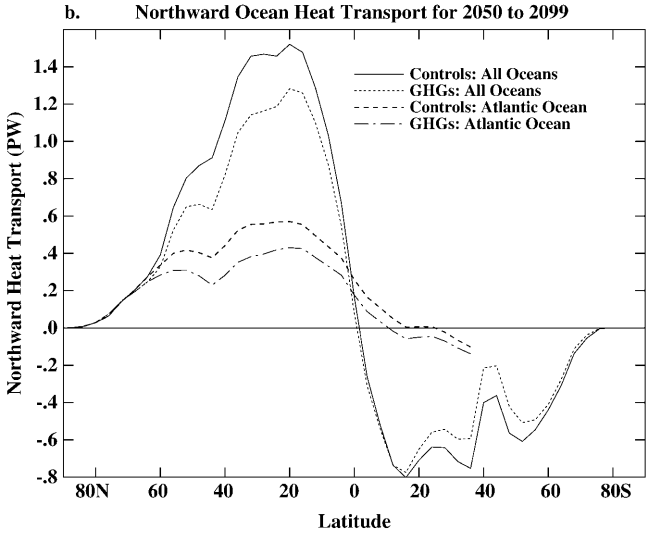

Fig. 4 **a** Change in surface heating into the oceans for 2050 to 2099 minus 1950 for the average of the two GHG experiments minus the control simulations as a function of latitude. **b** Northward ocean heat transport for 2050 to 2099 for the average of the two control simulations and for the average of the two GHG experiments

decrease and the specific volume to increase. This is discussed in greater detail in Miller and Russell (2000). Smaller rises occur near the Antarctic Circumpolar Current where heat is deposited into colder waters (reducing the expansion efficiency of heat) and where less ocean heat transport is received (due to a slowing of the ocean circulation as shown in Fig. 4b).

Figure 5 can be compared to Fig. 4 of Gregory and Lowe (2000). Both models show a smaller than average rise over the Antarctic Circumpolar Current. Unlike the present model, Gregory and Lowe (2000) do not show a sea level rise throughout the Arctic that exceeds the global average.

Figure 6 shows the model's projected sea level rise due to steric expansion for 2050 to 2099 minus 1950. It is calculated as the difference between the total sea level rise (Fig. 5) minus the rise due to water mass changes (Fig. 7) using the average of the two GHG experiments and the two control simulations. The steric expansion is small over shallow seas where there is less water to heat and over areas where the reduced ocean circulation is depositing less heat. The greatest increases occur in the deep basins of the Arctic Ocean due to less saline water.

Figure 6 can be compared to Fig. 3b of Bryan (1996) except that Bryan's calculation is performed over globally uniform pressures from 0 to 1130 db and ours is performed effectively over a time invariant spatially varying ocean column mass. Both models show the

greatest rise in the Arctic Ocean and smaller rises over the Antarctic Circumpolar Current. Our model shows less steric expansion over the continental shelves. Other regions show less extreme changes with mixed agreement.

6 Storage changes in water reservoirs

The atmosphere-ocean model does not include anthropogenic modifications of land hydrology, such as dams, river diversions, or ground water withdrawals, which may affect sea level (Gornitz et al. 1997). The glacial ice calving from Antarctica is constant in the model and cannot affect the model's sea level changes. However, the repartition of water among the model's reservoirs does cause sea level changes.

Figure 7 shows the model's projected ocean water mass changes for 2050 to 2099 minus 1950. High values occur over shallow ocean areas where steric expansion contributes a proportionally smaller share to global sea level, because of the thinner water column. Negative values occur, particularly in the deep areas of the Arctic Ocean, where increased freshwater input reduces the salinity and greater haline expansion is pushing mass out. For the Arctic as a whole, both steric expansion and water mass changes exceed those of the global oceans (Miller and Russell 2000).

Table 3 shows the mass changes in the model's water reservoirs for each 50-year period and for each GHG experiment minus its control simulation. Volumetric changes are calculated in units of global sea level rise (mm/year) by dividing the annual change in a reservoir (kg/year) by the product of density (1000 kg/m^3) times ocean and sea ice surface area ($361 \cdot 10^{12}$ m^2). As the climate warms, atmospheric water vapor, lake mass, and ocean mass increase at the expense of land ice and snow. Table 4 shows a breakdown of the land ice changes of Table 3 into different regions.

Figure 8 shows the changes in water or ice accumulation in the continental reservoirs for 2050 to 2099

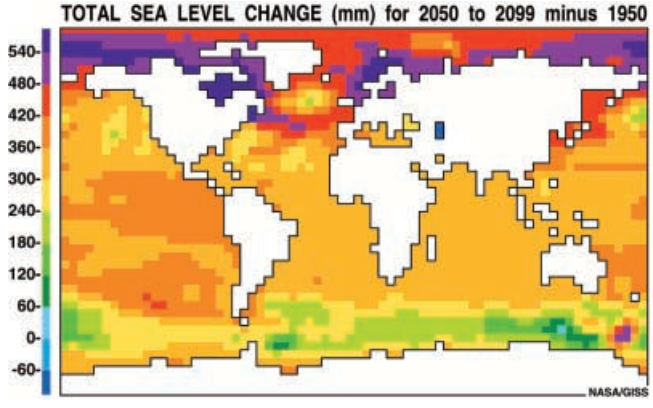

Fig. 5 Spatial distribution of total sea level change for 2050 to 2099 minus 1950 for the average of the two GHG experiments minus the control simulations

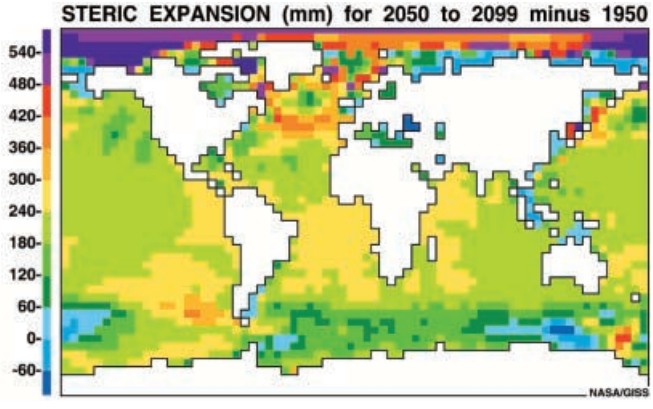

Fig. 6 Spatial distribution of steric expansion for 2050 to 2099 minus 1950 for the average of the two GHG experiments minus the control simulations

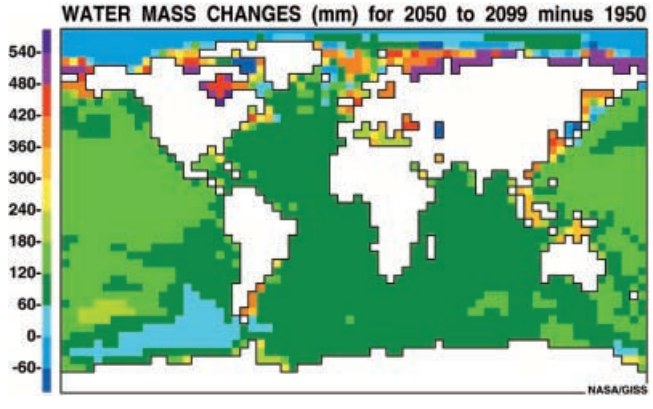

Fig. 7 Spatial distribution of ocean and sea ice mass changes for 2050 to 2099 minus 1950 for the average of the two GHG experiments minus the control simulations

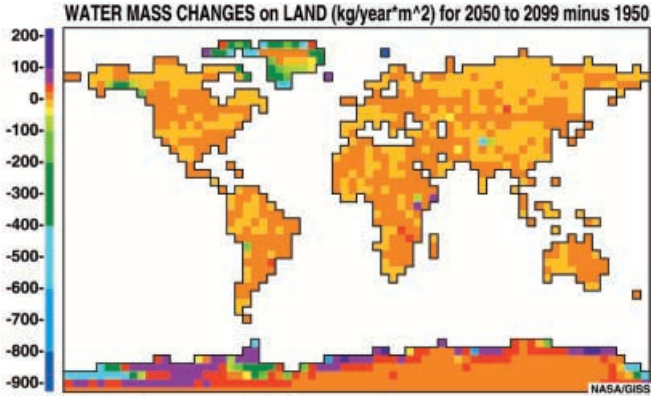

Fig. 8 Spatial distribution of continental water reservoir changes for 2050 to 2099 minus 1950 for the average of the two GHG experiments minus the control simulations

minus 1950. The net mass balance of land ice is negative in both hemispheres, on average: melting rapidly in the Northern Hemisphere but slowly in Antarctica as shown in Table 4. The coastal regions of Greenland are losing mass, even though precipitation is increasing almost everywhere there. Snow and ice are also melting in Alaska and the Himalayas. The high-altitude coastal regions and interior of Antarctica are slowly accumulating snow, whereas the ice shelves are melting rapidly.

There are significant changes in some grid cells that do not drain to the ocean. Lake Turkana in Kenya, Somalia, and western Mongolia are receiving more water in the GHG experiments, whereas Lakes Titicaca and Poopo in the Andes, the Aral Sea, Afghanistan, and southern Ethiopia are receiving less. There are also increasing lake levels in regions with slow moving rivers, namely Parana tributaries in southern Brazil, the Zambezi mouth, and the headwaters of the Zaire River. Changes at individual grid cells are uncertain; they should be checked with ground observations and other data.

7 Discussion

Four simulations of the NASA/GISS atmosphere-ocean model are used to emulate sea level changes between 1950 and 1998, and to project such changes to the year 2099. The only radiative forcing used is that of greenhouse gas changes: observed concentrations were used before 1991 and a compounded annual increase of 0.5% for CO_2 was used from 1991 to 2099. The simulations predict that global sea level will rise at a rate of 1.23 mm/year between 1950 and 1999, increasing to 2.97 between 2000 and 2049, and to 5.21 between 2050 and 2099. Because the GHG experiments are started from equilibrium, they underestimate the sea level rise that should have occurred in the real world since the real world was not in equilibrium in 1950. Observations indicate that during the past century sea level has risen between 1 and 2.5 mm/year (Warrick et al. 1996). Uncertainties in future greenhouse gas concentrations introduce uncertainties into the model's prediction of future sea level rise.

The surface air temperature changes of these simulations have been compared to observed temperature changes for the past 40 years and have been found to be reasonable both globally and regionally in the Northern Hemisphere (Russell et al. 2000). The thermal expansion component of sea level is controlled mainly by ocean surface fluxes and by ocean mixing both of which also affect the surface air temperature. Consequently, we expect the the ocean thermal expansion in the model to be reasonable.

Global thermal expansion rates from different one dimensional, two dimensional, and three dimensional models are difficult to compare. Ideally, model results on sea level rise should provide three key pieces of information on thermal expansion: the forcing scenario used, the amount of heat that entered the ocean, and the global sea level rise due to that heat. The second piece is often omitted, but were it to be provided (and it should be available), it would break a complex process into two simpler processes.

A new term, the "expansion efficiency of heat", which is the ratio of sea level rise due to thermal expansion divided by the heat entering the ocean, can be compared among different models. A high expansion efficiency indicates that heat is being distributed into warmer (surface, tropical) water and a low value indicates that heat is being distributed into colder (deeper, high latitude) water. Expansion efficiency of heat increases with temperature, pressure and salinity, and can be calculated from known ocean variables.

The present model's water mass changes are probably less reliable than its steric expansion. The model predicts increased snow fall on the ice sheets, with even greater melting around their edges, which seems reasonable. One large uncertainty is a possible change in glacial ice dynamics (such as a collapse of the West Antarctic ice sheet) which the model cannot simulate. A second large uncertainty is the correctness of the model's general circulation. Smaller sources of uncertainty lie in the model's fixed lake and glacial ice areas, the behavior of grid cells without a river outlet, the absence of dams, and ground water withdrawals.

As stated by Bryan (1996): "The most useful aspect of using a general circulation model of the ocean to estimate sea level rise is a prediction of the spatial distribution of the sea level rise." It appears that sea level will rise more rapidly in the Arctic Ocean (due to greater river flow and lower salinity) and more slowly along the Antarctic Circumpolar Current (where expansion by heat is less efficient) as shown by more than one model. Other regions show less extreme sea level changes and there is mixed agreement among the models.

Additional quantities and data of these simulations are available at our web site at: http://aom.giss.nasa.gov.

Acknowledgements Both Jonathan M. Gregory and Kirk Bryan made useful improvements to this paper. Jean A. Lerner assisted in creating the figures.

References

Abramopoulos F, Rosenzweig C, Choudhury B (1988) Improved ground hydrology calculations for global climate models (GCMs): soil water movements and evapotranspiration. J Clim 1: 921–941

Bryan K (1996) The steric component of sea level rise associated with enhanced greenhouse warming: a model study. Clim Dyn 12: 545–555

Cubasch U, Hegerl GC, Hellbach A, Hock H, Mikolajewicz U, Santer BD, Ross R (1995) A climate change simulation starting from 1935. Clim Dyn 11(2): 71–84

DeWolde JR, Huybrechts P, Oerlemans J, Van der Wal RSW (1997) Projections of global mean sea level rise calculated with a 2d energy-balance climate model and dynamic ice sheet models. Tellus 49A: 486–502

Fofonoff NP, Millard RC (1983) Computation of fundamental properties of seawater. UNESCO, Technical Papers in Marine Science 44

Gornitz V (1995a) Monitoring sea level changes. Clim Change 31: 515–544

Gornitz V (1995b) A comparison of differences between recent and late Holocene sea-level trends from eastern North America and other selected regions. J Coast Res Spec Iss 17: 287–297

Gornitz V, Lebedeff S (1987) Global sea level changes during the past century. In: Nummedal D, Pilkey OH, Howard JD (eds) Sea level fluctuations and coastal evolution. SEPM Spec Publ 41: 3–16

Gornitz V, Solow A (1991) Observations of long-term tide-gauge records for indicators of accelerated sea-level rise. In: Schlesinger ME (ed) Greenhouse-gas-induced climatic change: a critical appraisal of simulations and observations. Elsevier, Amsterdam, pp 347–367

Gornitz V, Rosenzweig C, Hillel D (1997) Effects of anthropogenic intervention in the land hydrologic cycle on global sea level rise. Glob Planet Change 14: 147–161

Gregory JM, Lowe JA (2000) Predictions of global and regional sea-level rise using AOGCMs with and without flux adjustment. Geophys Res Lett (in press)

Hansen JE, Sato M, Lacis A, Ruedy R, Tegan I, Matthews E (1998) Climate forcings in the industrial era. Proc Natl Acad Sci 95: 12 753–12 758

Houghton JT, Callander BA, Varney SK (eds) (1992) Climate change 1992: the supplementary report to the IPCC scientific Assessment. Cambridge University Press, Cambridge, UK, 200 pp

Houghton JT, Meira Filho LG, Callander BA, Harris N, Kattenberg A, Maskell K (eds) (1996) Climate change 1995: the science of climate change. Cambridge University Press, Cambridge, UK, 567 pp

Hurrell JW (1995) Decadal trends in the North Atlantic Oscillation: regional temperatures and precipitation. Science 269: 676–679

Komar PD, Enfield DB (1987) Short-term sea level changes and shore-line erosion. In: Nummedal D, Pilkey OH, Howard JD (eds) Sea level fluctuations and coastal evolution. SEPM Spec Publ 41: 17–27

Large WG, McWilliams JC, Doney SC (1994) Oceanic vertical mixing: review and a model with non-local boundary layer parameterization. Rev Geophys 32: 363–403

Levitus S, Burgett R, Boyer TP (1994) World ocean atlas 1994. US Department of Commerce, NOAA, Washington, DC, USA

Maul GA, Hanson K (1991) Interannual coherence between North Atlantic atmospheric surface pressure and composite southern USA sea level. Geophys Res Lett 18: 653–656

Miller JR, Russell GL (2000) Projected impact of climate change on the freshwater and salt budgets of the Arctic Ocean by a global climate model. Geophys Res Lett 27(8): 1183–1186

Nerem RS (1999) Measuring very low frequency sea level variations using satellite altimeter data. Glob Planet Change 20: 157–171

Peltier WR (1999) Global sea level rise and glacial isostatic adjustment. Glob Planet Change 20: 93–123

Peltier WR, Tushingham AM (1991) Global sea level rise and the greenhouse effect: might they be connected. Science 244: 806–810

Pirazzoli PA (1991) World atlas of Holocene sea-level changes. Elsevier, Amsterdam, 300 pp

Raper SCB, Wigley TML, Warrick RA (1996) Global sea-level rise: past and future. In: Milliman JD, Haq BU (eds) Sea level rise and coastal subsidence, causes, and consequences and strategies. Kluwer Academic Publishers, Dordrecht, 369 pp

Russell GL, Miller JR, Rind D, Ruedy RA, Schmidt GA, Sheth S (2000) Comparison of model and observed regional temperature changes during the past 40 years. J Geophys Res 105(D11): 14 891–14 898

Russell GL, Miller JR, Rind D (1995) A coupled atmosphere-ocean model for transient climate change studies. Atmos-Ocean 33(4): 683–730

Spencer NE, Woodworth PL (1993) Data holdings of the Permanent Service for Mean Sea Level. PSMSL, Bidston Observatory, Birkenhead, UK, 81 pp

Warrick RA, LeProvost C, Meier MF, Oerlemans J, Woodworth PL (1996) In: Houghton JT, Meira Hilho LG, Callander BA, Harris N, Kattenberg A, Maskell K (eds) Climate change 1995: the science of climate change. Cambridge University Press, Cambridge, UK, 567 pp